# **BMC Medical Genomics**

# Identifying genetic markers enriched by brain imaging endophenotypes in Alzheimer's disease

--Manuscript Draft--

Manuscript Number:	MGNM-D-22-00298						
Full Title:	Identifying genetic markers enriched by brain imaging endophenotypes in Alzheimer's disease						
Article Type:	BMC Supplements Reviewed						
Section/Category:	Bioinformatic and algorithmical studies						
Funding Information:	U.S. National Library of Medicine (R01 LM013463)	Dr Li Shen					
	national institute on aging (U01 AG068057)	Dr Li Shen					
	national institute on aging (R01 AG058854)	Dr Li Shen					
	Directorate for Computer and Information Science and Engineering (IIS 1837964)	Dr Li Shen					
	National Research Foundation of Korea (NRF-2020R1A6A3A03038525)	Dr. Mansu Kim					
	national institute on aging (P30 AG010133)	Dr. Andrew J Saykin					
	national institute on aging (R01 AG071470)	Dr Li Shen					
	from 60% to 80%. The most straightforward genetic basis is to perform genome-wide as diagnostic status. These GWAS studies has susceptibility loci. Recently, imaging genetic imaging measures are studied as quantitatic Given that many imaging genetics studies of analysis, the identified imaging or genetic nodisease outcome. Results: We propose a genetic variants enriched by imaging endopeassociated with both genetic factors and dissteps: 1) map the effects of a genetic variant SNP) onto imaging traits across the brain undeffects of a diagnosis phenotype onto imaging regression model, and 3) detect SNP-diagneffects with the diagnostic effects on the brain undeffects with the diagnostic effects on the brain intitative (ADNI) database. Among 54 AD real large-scale AD GWAS, our approach identic cohort while the standard association approach the proposed imaging endophenotype enricegenetic variants undetectable using the tracegrous proposed a novel method to identify AD general succession in the proposed and the proposed in the proposed in the proposed in the proposed and the proposed in the	Background: Alzheimer's Disease (AD) is a complex neurodegenerative disorder and the most common type of dementia. AD is characterized by a decline of cognitive function and brain atrophy, and is highly heritable with estimated heritability ranging from 60% to 80%. The most straightforward and widely used strategy to identify AD genetic basis is to perform genome-wide association study (GWAS) of the case-control diagnostic status. These GWAS studies have identified over 50 AD related susceptibility loci. Recently, imaging genetics has emerged as a new field where brain imaging measures are studied as quantitative traits (QTs) to detect genetic factors. Given that many imaging genetics studies did not involve the diagnostic outcome in the analysis, the identified imaging or genetic markers may not be related or specific to the disease outcome. Results: We propose a novel method to identify disease-related genetic variants enriched by imaging endophenotypes, which are the imaging traits associated with both genetic factors and disease status. Our analysis consists of three steps: 1) map the effects of a genetic variant (e.g., single nucleotide polymorphism or SNP) onto imaging traits across the brain using a linear regression model, 2) map the effects of a diagnosis phenotype onto imaging traits across the brain using a linear regression model, and 3) detect SNP-diagnosis association via correlating the SNP effects with the diagnostic effects on the brain-wide imaging traits. We demonstrate the promise of our approach by applying it to the Alzheimer's Disease Neuroimaging Initiative (ADNI) database. Among 54 AD related susceptibility loci reported in prior large-scale AD GWAS, our approach identifies 41 of those from a much smaller study cohort while the standard association approaches identify only two of those. Clearly, the proposed imaging endophenotype enriched approach can reveal promising AD genetic variants undetectable using the traditional method. Conclusion: We have proposed a novel method to identify A					
Corresponding Author:	Li Shen University of Pennsylvania Perelman School Philadelphia, PA UNITED STATES	ol of Medicine					
O a management of the second o	li.shen@pennmedicine.upenn.edu						
Corresponding Author E-Mail:	ii.snen@pennmedicine.upenn.edu						

Information:	
Corresponding Author's Institution:	University of Pennsylvania Perelman School of Medicine
Corresponding Author's Secondary Institution:	
First Author:	Mansu Kim, Ph.D.
First Author Secondary Information:	
Order of Authors:	Mansu Kim, Ph.D.
	Ruiming Wu
	Xiaohui Yao, Ph.D.
	Andrew J Saykin, Psy.D.
	Jason H Moore, Ph.D.
	Li Shen, Ph.D.
Order of Authors Secondary Information:	
Opposed Reviewers:	
Additional Information:	
Question	Response
Has this manuscript been submitted before to this journal or another journal in the <a href="https://www.biomedcentral.com/p/th e-bmc-series-journals#journallist" target="_blank">BMC series</a> / a>?	Yes
Please provide the manuscript identification number from your previous submission. submission. f you no longer have the identification number, please specify this in the text box below. br/> emsp; as follow-up to "Has this manuscript been submitted before to this journal or another journal in the <a href="https://www.biomedcentral.com/p/the-bmc-series-journals#journallist" target="_blank">BMC series</a>	SUPP-D-21-00200R3

## **RESEARCH**

# Identifying genetic markers enriched by brain imaging endophenotypes in Alzheimer's disease

Mansu Kim<sup>1</sup>, Ruiming Wu<sup>2</sup>, Xiaohui Yao<sup>3</sup>, Andrew J. Saykin<sup>4</sup>, Jason H. Moore<sup>5</sup>, Li Shen<sup>3\*</sup> and for the Alzheimer's Disease Neuroimaging Initiative<sup>6</sup>

### **Abstract**

Background: Alzheimer's Disease (AD) is a complex neurodegenerative disorder and the most common type of dementia. AD is characterized by a decline of cognitive function and brain atrophy, and is highly heritable with estimated heritability ranging from 60% to 80%. The most straightforward and widely used strategy to identify AD genetic basis is to perform genome-wide association study (GWAS) of the case-control diagnostic status. These GWAS studies have identified over 50 AD related susceptibility loci. Recently, imaging genetics has emerged as a new field where brain imaging measures are studied as quantitative traits (QTs) to detect genetic factors. Given that many imaging genetics studies did not involve the diagnostic outcome in the analysis, the identified imaging or genetic markers may not be related or specific to the disease outcome.

Results: We propose a novel method to identify disease-related genetic variants enriched by imaging endophenotypes, which are the imaging traits associated with both genetic factors and disease status. Our analysis consists of three steps: 1) map the effects of a genetic variant (e.g., single nucleotide polymorphism or SNP) onto imaging traits across the brain using a linear regression model, 2) map the effects of a diagnosis phenotype onto imaging traits across the brain using a linear regression model, and 3) detect SNP-diagnosis association via correlating the SNP effects with the diagnostic effects on the brain-wide imaging traits. We demonstrate the promise of our approach by applying it to the Alzheimer's Disease Neuroimaging Initiative (ADNI) database. Among 54 AD related susceptibility loci reported in prior large-scale AD GWAS, our approach identifies 41 of those from a much smaller study cohort while the standard association approaches identify only two of those. Clearly, the proposed imaging endophenotype enriched approach can reveal promising AD genetic variants undetectable using the traditional method.

Conclusion: We have proposed a novel method to identify AD genetic variants enriched by brain-wide imaging endophenotypes. This approach can not only boost detection power, but also reveal interesting biological pathways from genetic determinants to intermediate brain traits and to phenotypic AD outcomes.

Keywords: Brain imaging genetics; Genome-wide association study; Imaging-diagnosis map; Imaging-genetics map

# Background

Alzheimer's Disease (AD) is a complex neurodegenerative disorder, and the most common type of dementia [1]. Today, approximately 5.8 million people are suffering from AD-related dementia in the United States, and it is expected to exceed 13.8 million by 2050 [2]. AD is characterized by a decline of cognitive function and brain atrophy, and it is highly heritable with estimated heritability ranging from 60% to 80% [3]. The most straightforward and widely

used strategy to identify AD-related genetic markers such as single-nucleotide polymorphisms (SNPs) is to perform genome-wide association studies (GWAS) or GWAS-based meta-analyses on a case-control diagnostic phenotype. Using this strategy, recent studies (e.g., [1, 4, 5]) have identified over 50 AD related susceptibility loci. This method faces a major burden for multiple comparison correction and thus requires a large sample size to detect SNPs with small effect sizes.

To address this challenge, imaging genetics [6] is emerging as a new promising field, where imaging quantitative traits (QTs) are used as phenotypes to identify relevant genetic markers. Of note, imaging

 $<sup>^*</sup>$ Correspondence: li.shen@pennmedicine.upenn.edu

<sup>&</sup>lt;sup>3</sup>Department of Biostatistics, Epidemiology and Informatics, Perelman School of Medicine at the University of Pennsylvania, Philadelphia, USA Full list of author information is available at the end of the article

Kim et al. Page 2 of 11

QTs are quantitative measures, statistically more powerful than binary case-control status, and thus have greater potential to identify subtle genetic signals with small effect sizes from study cohorts of moderate sample sizes [7]. For example, Shen et al. [8] used cortical thickness, volume, and gray matter density measures as QTs to examine genetic effects in AD. Given that many imaging genetics studies did not involve the diagnostic outcome directly in the analyses, the identified imaging or genetic markers may not be related or specific to disease outcomes such as AD.

To bridge this gap, we propose an innovative method to identify disease-related genetic variants enriched by imaging endophenotypes, which are the imaging traits associated with both genetic factors and disease status. We demonstrate the promise of our method by applying it to the Alzheimer's Disease Neuroimaging Initiative (ADNI) database [9]. Our major contributions are twofold: 1) We propose a novel approach to identify AD genetic variants enriched by brain-wide imaging endophenotypes. This approach can not only boost detection power, but also reveal interesting biological pathways from genetic determinants to intermediate brain traits and then to phenotypic AD outcomes. 2) We show the effectiveness of our approach in an empirical study to link genetics with three disease outcomes (i.e., early mild cognitive impairment (EMCI), late MCI (LMCI), and AD) via mapping and correlating their associations with region-based amyloid imaging QTs across the brain.

## Results

We first report the results of our first experiment. In this experiment, to demonstrate the promise of our approach, we performed a comparative study with a few conventional genetic association methods. The benchmark algorithms used in this work include: 1) conventional GWAS analysis controlled for relevant covariates including age, sex and education (implemented in PLINK v1.90), 2) Pearson's correlation analysis between each SNP and each diagnosis outcome, and 3) the partial correlation analysis between each SNP and each diagnosis outcome while controling for relevant covariates. We performed empirical comparison on the real imaging genetics data from the ADNI cohort. On the genetics side, we analyzed 54 AD SNPs identified in recent landmark AD GWAS studies [1, 4, 5]. On the imaging QT side, we analyzed the AV-45 PET data due to its high sensitivity and specificity for distinguishing AD from MCI and CN [10, 11]. Three casecontrol comparisons (i.e., CN vs EMCI, CN vs LMCI, CN vs AD) were studied to explore imaging genetic effects on different disease stages.

# Identification of genetic variants associated with diagnosis based on GWAS analysis

Conventional GWAS analysis was applied to identify genetic variants for three diagnostic outcomes (i.e., CN vs AD, CN vs LMCI, and CN vs EMCL), respectively. After Bonferroni correction, we observed 1) APOErs429358 (corrected- $p=6.23\times10^{-13}$ ) and PVRL2rs41289512 (corrected- $p=2.09\times10^{-4}$ ) were significantly associated with AD diagnosis, and 2) APOErs429358 (corrected- $p=2.51\times10^{-3}$ ) was also significantly associated with LMCI diagnosis. No significant SNPs were identified to be associated with EMCI diagnosis. Table 1 shows the detailed results.

# Identification of genetic variants associated with diagnosis based on correlation analysis

The Pearson's correlation and partial correlation analyses were applied to identify genetic variants related to three diagnostic outcomes. These two correlation analyses yielded very similar genetic findings. The detailed results are shown in Table 1 and Table 2.

For Pearson's correlation analysis, we observed that APOE-rs429358 was significantly correlated with all three diagnoses (i.e., r=0.42 and corrected- $p=1.15\times 10^{-18}$  for AD diagnosis, r=0.18 and corrected- $p=5.40\times 10^{-3}$  for LMCI diagnosis, and r=0.26 and corrected- $p=1.04\times 10^{-6}$  for EMCI diagnosis), and PVRL2-rs41289512 was significantly correlated with AD diagnosis (r=0.22 and corrected- $p=2.75\times 10^{-4}$ ).

For partial correlation analysis, we observed that APOE-rs429358 was significantly correlated with all three diagnoses (i.e., r=0.44 and corrected- $p=1.20\times 10^{-20}$  for AD diagnosis, r=0.28 and corrected- $p=6.15\times 10^{-8}$  for LMCI diagnosis, and r=0.20 and corrected- $p=2.32\times 10^{-4}$  for EMCI diagnosis), and PVRL2-rs41289512 was significantly correlated with AD diagnosis (r=0.23 and corrected- $p=6.66\times 10^{-5}$ ).

# Identification of genetic variants associated with diagnosis via correlating their effect maps on brain Step 1. Imaging-diagnosis association analysis

The linear regression model was applied to examine the diagnostic effect on AV-45 imaging QTs. Figure 1 shows the resulting p-value maps for three comparisons (i.e., CN vs EMCI, CN vs LMCI, CN vs AD), where  $-log_{10}(p)$  values are shown. On average, CN vs AD yielded the most significant diagnostic effects on imaging QTs, and CN vs EMCI yielded the least significant ones. This matches our intuition about the abnormality change of the amyloid imaging QTs over the disease progression. Table 3 shows the top 10 significant regions for the three analyses. Eight regions are common across the three disease stages, including left and right medial orbital superior frontal gyrus, rectus and middle orbital frontal gyrus, right superior orbital frontal gyrus, and left middle temporal gyrus.

65

Kim et al. Page 3 of 11

### Step 2. Imaging-genetics association analysis

We performed an univariate imaging genetics analysis to examine genetic effects of each studied SNP on each AV-45 imaging QT. Figure 1 shows the resulting p-value maps for three groups (i.e., CN vs EMCI, CN vs LMCI, CN vs AD), where  $-log_{10}(p)$  values are shown. The imaging genetic patterns appear to be similar among these three groups, while CN vs AD and CN vs LMCI yielded slightly stronger imaging genetic associations than CN vs EMCI. In all three cases, APOE-rs429358 and PVRL2-rs41289512 have significant effects on most of the ROIs. Specifically, most of the 116 brain ROIs (i.e., 97 ROIs for CN vs AD, 98 ROIs for CN vs LMCI, and 89 ROIs for CN vs EMCI) were significantly associated with APOErs429358. The PVRL2-rs41289512 had significant genetic effects on 79 ROIs for CN vs AD, 68 ROIs for LMCI vs AD, and 65 ROIs for CN vs EMCI. The full list of SNP-ROI findings for the three comparisons are available in Supplementary Table S1 of "Additional File 1".

# Step 3. Correlation analysis between brain maps of diagnostic effect vs genetic effect

After estimating genetic and diagnostic effects on the AV-45 imaging QTs, we performed the Pearson's correlation analysis to identify the genetic variants associated with the diagnosis outcomes via correlating the genetic and diagnostic maps in the brain. In Table 2 and Table 1, we observed that APOE-rs429358 obtained the highest correlations with all three diagnoses (i.e., r = 0.88 and corrected- $p = 1.35 \times$  $10^{-36}$  for AD diagnosis, r = 0.90 and corrected-p = $1.99 \times 10^{-41}$  for LMCI diagnosis, and r = 0.88 and corrected- $p = 1.53 \times 10^{-35}$  for EMCI diagnosis), and PVRL2-rs41289512 obtained the second highest correlations (i.e., r = 0.80 and corrected- $p = 5.82 \times$  $10^{-25}$  for AD diagnosis, r = 0.74 and corrected-p = $1.72 \times 10^{-19}$  for LMCI diagnosis, and r = 0.86 and corrected- $p = 1.33 \times 10^{-33}$  for EMCI diagnosis). According to Table 2 and Table 1, we observed that our newly proposed method identified a lot more significant SNPs in all three comparisons than the convectional GWAS and Pearson's correlation and partial correlation analyses. This shows the promise of our method, which identifies SNP-diagnosis associations through mapping their effects on the imaging QTs across the brain. Many of these QTs can serve as endophenotypes linking genetic factors to disease outcomes. This approach can not only boost detection power, but also reveal interesting biological pathways from genetic determinants to intermediate brain traits and to phenotypic AD outcomes.

## Comparison with analyzing "non-AD" SNPs

Now we report the results of our second experiment, which is designed to compare the findings between the analysis of the above 54 AD susceptibility loci versus the analysis of a same number of random "non-AD" SNPs that have not been linked to AD before. As mentioned in the "Methods" section, we ran our pipeline 10,000 times, and each time it was applied to 54 randomly selected "non-AD" SNPs. Figure 2 shows the distribution of the number of significant findings across these 10,000 analyses on the random "non-AD" SNPs. For comparison purposes, the number of significant findings from analyzing the 54 AD susceptibility loci is plotted as a red dash line in Figure 2; and the details of these findings are shown in Table 1. Specifically, using this pipeline, our analysis on 54 AD susceptibility loci yielded 19 findings for the CN vs AD comparison, which outperformed 86.88% analyses on the random "non-AD" SNPs (Figure 2(a)); yielded 28 findings for the CN vs LMCI comparison, which outperformed 99.35% analyses on the random "non-AD" SNPs (Figure 2(b)); and yielded 20 findings for the CN vs EMCI comparison, which outperformed 81.45% analyses on the random "non-AD" SNPs (Figure 2(c)). These findings indicate that our pipeline has a higher probability to identify AD susceptibility loci than random SNPs that have not vet been linked to AD before. Of note, our pipeline is not designed to directly examine SNP-diangosis associations. However, the above observation demonstrates the promise of our proposed strategy to identify AD-related SNPs through mapping brain imaging endophenotypes.

### Discussion

A major challenge in AD genetics is how to effectively detect weak signals such as SNPs with small effect sizes. Various strategies have been proposed to increase detection power in genetic association studies [6]. For example, one approach could be to focus on analyzing a small number of prioritized SNPs with relevant functional annotation (e.g., those from the amyloid pathway, or expression QT loci related to brain tissues) to reduce burden for multiple comparison correction. Another approach could be to use enrichment analysis to look for stronger collective effects at the pathway or network level instead of the individual effect from each single SNP.

In this work, we have proposed an innovative pipeline to identify interesting SNP-disease associations supported or enriched by the intermediate imaging QTs (endophenotypes) across the entire brain. To the best of our knowledge, this is the first approach to enrich genetic variants associated with AD via mapping their association patterns with imaging QTs in the brain. In

Kim et al. Page 4 of 11

our empirical study on the ADNI data, we confirmed multiple genetic variants estimated by conventional models, such as APOE (corrected- $p = 1.35 \times 10^{-36}$ ) rs429358) and PVRL2 (corrected- $p = 5.82 \times 10^{-25}$ , rs41289512), as well as other AD-related genetic variants shown in Table 2 and Table 1. Furthermore, we demonstrated our analysis could identify a lot more SNPs than conventional approaches. In addition, the significant imaging QTs identified in Figures 1-3 have the potential to serve as imaging endophenotypes linking the genetic variant with the disease outcome.

The traditional strategy for identifying genetic variants related to diagnosis is GWAS analysis, which tests the effect of SNP on the diagnostic outcome. Although it has been widely used, a conventional GWAS analysis does not have enough power to identify weak signals from moderately sized study samples. Joint mapping of SNP and diagnostic effects via neuroimaging data, which provide quantifiable traits of disease, can potentially reveal new insights to identify weak but meaningful endophenotype-backed genetic signals for the disease outcome. Compared to traditional strategy, our approach obtained much stronger signals of significance as well as correlation coefficients and identified a lot more interesting genetic variants missed by traditional methods, as shown in Table 1. For example, our approach yielded a much more significant APOE-rs429358 signal than traditional methods. Even though all 54 SNPs have been associated with AD in prior large-scale GWAS studies, applying traditional methods to our moderately sized ADNI sample only yielded two significant SNPs. However, using the proposed method, we obtained 41 significant SNPs. These findings suggest that the proposed method has the potential to boost the detection power.

In our analysis, the following 16 SNPs were found significantly correlated with two or three diagnostic outcomes: rs4574098, rs35349669, rs6448453, rs2718058, rs1859788, rs1476679, rs12539172, rs867611, rs17125924, and rs6024870. Furthermore, the following five SNPs were significant and positively correlated with all diagnosis outcomes: rs9271058, rs3752246, rs4147929, rs41289512, and rs429358. These identified SNPs have the same sign of correlation coefficients. Our findings are in accordance with previous studies [12, 13, 14, 15, 16, 17, 18, 19, 20]. For example, rs9271058 was associated with higher expression levels of HLA-DRB1 in various brain regions [15]. The rs3752246 G allele carriers were observed to have an increased risk for developing AD considering C/C genotype as reference category [21]. A recent study showed that the rs4147929 variant minor A allele could significantly increase ABCA7 expression, and ABCA7 showed significantly increased gene expression in AD patients

compared with controls [22]. These findings demonstrate the effectiveness of our model on identifying biologically meaningful genetic findings.

Interestingly, we found that only one SNP (i.e., CD33, rs3865444) reported mixed signs of correlation coefficients (i.e., -0.40 for AD diagnosis, 0.45 for LMCI diagnosis, -0.41 for EMCI diagnosis). A previous study showed a bidirectional modulation of CD33 genotype associated cognitive performance [23]. The CD33 genotype had a positive correlation with cognitive function than the CD33 when the precuneus gFCD is lower than 0.04 a. However, the relationship became negative when gFCD in precuneus increased to 0.58. With these observations, it warrants further investigation on independent cohorts to have a better understanding of the mixed directionality on the association between CD33 rs3865444 and different diagnostic stages.

In our second experiment, we performed comparative studies through applying the proposed pipeline to random "non-AD" SNPs. It is promising that our pipeline has been able to to identify a lot more AD susceptibility loci than random SNPs that have not yet been linked to AD before. However, these random SNP analyses have also yielded some significant findings, which warrant further investigation towards a few interesting directions. First, some of these findings could be true signals missed by the existing studies (e.g., due to small effect sizes). Thus, our findings could provide valuable guidance for subsequent replication studies in independent cohorts. Second, some of the findings may not have a direct effect on the diagnosis. However, by the design of our pipeline, these findings are indirectly connected to the diagnostic phenotype via being related to a same set of imaging endophenotypes. Such a mechanism warrants a more detailed further investigation. Third, some of these findings could be false discoveries. One potential limitation of our method is that we include all the ROIs in the brain while correlating the genetic map with the diagnostic map. It rs17125944, rs12590654, rs28394864, rs28394864, rs601472is likely that some ROIs are irrelevant to the pathway from genetics to phenotypical outcomes. They may introduce noises and biases, leading to possible false discoveries. Thus, an interesting future direction could be to identify only relevant ROIs for mapping genetic and diagnostic effects. Another interesting direction could be to explore different and improved mapping strategies. For example, the current pipeline employs a linear regression model in both Step 1 and Step 2. This simple modeling strategy coupled with the existence of irrelevant ROIs could lead to false positive or negative discoveries. Expanding to a nonlinear model, such as polynomial regression or a fully connected neural network model, has the potential to capture complex associations and improve biomarker identification. This remains as an interesting future topic to explore.

Kim et al. Page 5 of 11

## **Conclusion**

We have proposed an innovative method to identify disease-related genetic variants enriched by imaging endophenotypes, which are the imaging quantitative traits (QTs) associated with both genetic factors and disease status. Our approach consists of three steps: 1) association analysis between imaging QTs and diagnosis, 2) association analysis between imaging QTs and each genetic variant, and 3) correlation analysis between two brain maps produced in Step 1 (i.e., map of diagnostic effect) and Step 2 (i.e., map of genetic effect). We applied our method to the ADNI cohort to identify genetic markers enriched by amyloid imaging endophenotypes in AD. Among 54 AD related susceptibility loci reported in prior large-scale AD GWAS, our approach identified 41 of those from a much smaller study cohort (i.e., ADNI) while the standard genetic assocation approaches identified only two of those. Our method yielded not only a lot more AD genetic variants undetectable using the traditional method but also a set of imaging QTs significantly associated with both the genetic variant and the diagnostic outcome. Such QTs have the potential to serve as imaging endophenotypes linking genetics with AD outcomes. These promising findings demonstrate that our approach can not only boost detection power, but also provide valuable information for revealing interesting biological pathways from genetics to brain traits and to AD outcomes. An interesting future topic is to perform an in-depth investigation to explore the detailed relationships between the identified genetic markers and brain imaging traits for different disease stages.

### Methods

### Data description

Data used in the preparation of this article were obtained from the ADNI database (adni.loni.usc.edu) [9]. The ADNI was launched in 2003 as a public-private partnership, led by Principal Investigator Michael W. Weiner, MD. The primary goal of ADNI has been to test whether serial magnetic resonance imaging (MRI), positron emission tomography (PET), other biological markers, and clinical and neuropsychological assessment can be combined to measure the progression of MCI and early AD. For up-to-date information, see www.adni-info.org. In this work, participants (N=971) include 202 AD, 218 LMCI, 296 EMCI, and 255 cognitively normal (CN) subjects with complete baseline data including [18F]florbetapir (AV-45) PET scans (measuring amyloid burden), genotyping data, demographic information, and clinical assessments downloaded from the ADNI database (adni.loni.usc.edu). Demographic and clinical assessments of the participants are shown in Table 4.

### Data preprocessing

Preprocessed AV-45 PET scans are collected and aligned to the Montreal Neurological Institute space as  $2\times2\times2$  mm voxels. Standard uptake value ratio is computed by intensity normalization based on a cerebellar crus reference region. We then extract regional neuroimaging measurements from 116 regions-of-interests (ROIs) based on the automated anatomical labeling (AAL) atlas. The genotyping data are downloaded and analyzed using PLINK v1.90 [24]. We perform quality control using the following criteria: genotyping call rate > 95\%, minor allele frequency > 5\%, and Hardy Weinberg Equilibrium  $> 1.00 \times 10^{-6}$ . Then, we select 54 susceptibility loci identified by recent AD GWAS or GWAS meta-analysis [1, 4, 5]. The full list of susceptibility loci are shown in Table 5. In addition, we also perform some comparison analyses on "non-AD" related SNPs, which are randomly selected from loci with p-values larger than 0.05 using the summary statistics in a recent landmark AD GWAS study [1].

# Proposed pipeline for linking SNPs with diagnosis via mapping their regional associations with amyloid imaging QTs across the brain.

The proposed pipeline aims to identify genetic markers enriched by amyloid imaging endophenotypes in AD. The pipeline consists of three steps: 1) association analysis between imaging QTs and diagnosis, 2) association analysis between imaging QTs and each genetic variant, and 3) correlation analysis between two brain maps produced in Step 1 (i.e., map of diagnostic effect) and Step 2 (i.e., map of genetic effect).

### Step 1. Imaging-diagnosis association analysis

Let x be a diagnostic outcome (i.e., case vs control) and Y be a set of AV-45 imaging QTs. We perform the following simple linear regression model to examine the diagnostic effect on each imaging QT  $y \in Y$ .

$$y = \beta x + \Gamma Z + \epsilon, \tag{1}$$

where  $Z = (z_1, \dots, z_k)^T$  includes the variables whose effects we want to exclude, such as age, sex, and education;  $\beta$  and  $\Gamma = (\gamma_1, \dots, \gamma_k)$  are the coefficients; and  $\epsilon$  is the error term. Our goal is to estimate  $\beta$  and also test if the diagnosis x has a significant effect (i.e.  $\beta \neq 0$ ) on each QT  $y \in Y$ . As a result, we generate an ROI-based p-value map to quantify the significance of diagnostic effect on imaging data. In this work, each element of the significance map records the "negative log p-value"  $-loq_{10}(p)$  at the corresponding ROI.

Kim et al. Page 6 of 11

Step 2. Imaging-genetics association analysis Let G be a set of SNPs and Y be a set of AV-45 imaging QTs. We perform a linear regression model to estimate the additive effect of each SNP  $g \in G$  on each QT  $g \in Y$ . The analysis is performed for all possible SNP-QT pairs, and thus is repeated  $54 \times 116 = 6,264$  times. The linear regression model is defined as follows.

$$y = \alpha g + \Gamma Z + \epsilon, \tag{2}$$

where  $Z=(z_1,\cdots,z_k)^T$  includes the variables whose effects we want to exclude, such as age, sex, and education;  $\alpha$  and  $\Gamma=(\gamma_1,\cdots,\gamma_k)$  are the coefficients; and  $\epsilon$  is the error term. Our goal is to estimate  $\alpha$  and also test if the SNP g has a significant effect (i.e.  $\alpha \neq 0$ ) on each QT  $g \in Y$ .

Thus, we generate an ROI-based p-value map to quantify the significance of genetic effects on imaging data. Specifically, in this work, each element of the significance map records the "negative log p-value"  $-log_{10}(p)$  at the corresponding ROI.

Step 3. Correlation analysis between two brain maps (i.e., diagnostic effect vs genetic effect) In this step, the correlation analysis is applied to score the similarity between two significance maps generated in Steps 1-2. Specifically, Step 1 results in a brain map of the significance level for diagnostic effects in the format of  $-log_{10}(p)$ , and Step 2 results in multiple brain maps (one for each SNP) containing the significance level for genetic effects in the format of  $-log_{10}(p)$ . We perform Pearson's correlation analysis between these two maps to score their similarity. To identify significant correlations, we employ the Bonferroni method to correct for multiple comparison.

## Empirical study on the ADNI data

We conduct an empirical study on the ADNI data to evaluate the promise of the proposed pipeline for identifying novel SNPs related to AD. Our study includes two experiments. In the first experiment, we perform a targeted analysis on 54 AD susceptibility loci (see Table 5) using the proposed pipeline. We compare our findings with those derived from conventional genetic association methods. In the second experiment, we perform a comparative study exploring a same number of randomly selected "non-AD" SNPs that have not yet been linked to AD previously. Specifically, we randomly select 54 "non-AD" SNPs (i.e., p > 0.05) based on the summary statistics of a landmark AD genetics study [1], apply our pipeline to this SNP set, and report the number of significant findings. We repeat the above analysis 10,000 times with a different set of 54 randomly selected "non-AD" SNPs in each analysis, and report the distribution of the number of significant findings across all these analyses. We compare the number of significant findings from analyzing 54 AD susceptibility loci (see Table 5) in the first experiment with those from analyzing random "non-AD" SNPs in the second experiment.

#### Acknowledgements

Data collection and sharing for this project was funded by the Alzheimer's Disease Neuroimaging Initiative (ADNI) (National Institutes of Health Grant U01 AG024904) and DOD ADNI (Department of Defense award number W81XWH-12-2-0012). ADNI is funded by the National Institute on Aging, the National Institute of Biomedical Imaging and Bioengineering, and through generous contributions from the following: AbbVie. Alzheimer's Association; Alzheimer's Drug Discovery Foundation; Araclon Biotech; BioClinica, Inc.; Biogen; Bristol-Myers Squibb Company; CereSpir, Inc.; Cogstate; Eisai Inc.; Elan Pharmaceuticals, Inc.; Eli Lilly and Company; Eurolmmun; F. Hoffmann-La Roche Ltd and its affiliated company Genentech, Inc.; Fujirebio; GE Healthcare; IXICO Ltd.; Janssen Alzheimer Immunotherapy Research & Development, LLC.; Johnson & Johnson Pharmaceutical Research & Development LLC.; Lumosity; Lundbeck; Merck & Co., Inc.; Meso Scale Diagnostics, LLC.; NeuroRx Research; Neurotrack Technologies; Novartis Pharmaceuticals Corporation; Pfizer Inc.; Piramal Imaging; Servier; Takeda Pharmaceutical Company; and Transition Therapeutics. The Canadian Institutes of Health Research is providing funds to support ADNI clinical sites in Canada. Private sector contributions are facilitated by the Foundation for the National Institutes of Health (www.fnih.org). The grantee organization is the Northern California Institute for Research and Education, and the study is coordinated by the Alzheimer's Therapeutic Research Institute at the University of Southern California. ADNI data are disseminated by the Laboratory for Neuroimaging at the University of Southern California.

### Funding

This work and publication costs were supported by the National Institutes of Health [R01 LM013463, U01 AG068057, R01 AG071470, R01 AG058854, P30 AG010133] and the National Science Foundation [IIS 1837964]. The work was also supported in part by the National Research Foundation of Korea [NRF-2020R1A6A3A03038525]. The funders were not involved in the design of the study and collection, analysis, and interpretation of data and in writing the manuscript.

### **Abbreviations**

Alzheimer's disease (AD); genome-wide association study (GWAS); single-nucleotide polymorphism (SNP); Alzheimer's Disease Neuroimaging Initiative (ADNI); quantitative trait (QT); early mild cognitive impairment (EMCI); late mild cognitive impairment (LMCI); cognitively normal (CN)

### Availability of data and materials

The datasets used and analyzed during the study are available in the ADNI LONI repository,  $\frac{1}{2}$ 

### Ethics approval and consent to participate

This research is conducted under the regulation of Institutional Review Boards (IRB) and the research subject informed consent process at University of Pennsylvania, USA. Study subjects gave written informed consent at the time of enrollment for data collection and completed questionnaires approved by each participating site's IRB. The authors state that they have obtained approval from the Alzheimer's Disease Neuroimaging Initiative (ADNI) Data Sharing and Publications Committee for use of the data.

### Competing interests

The authors declare that they have no competing interests.

### Consent for publication

Not applicable. Secondary analysis of publicly available data

65

Kim et al. Page 7 of 11

### Authors' contributions

MS, RW, AJS, JHM and LS: conceptualization and study design. MS and XY: data preparation and processing, MS and RW: method implementation and data analysis. MS and LS: drafting manuscript. All the authors reviewed, commented, revised and approved the manuscript.

#### Author details

<sup>1</sup>Department of Artificial intelligence, Catholic University of Korea, Bucheon, Republic of Korea. <sup>2</sup>School of Engineering and Applied Science, University of Pennsylvania, Philadelphia, USA. <sup>3</sup>Department of Biostatistics, Epidemiology and Informatics, Perelman School of Medicine at the University of Pennsylvania, Philadelphia, USA. <sup>4</sup>Indiana Alzheimer Disease Center and Department of Radiology and Imaging Sciences, Indiana University School of Medicine, Indianapolis, USA. <sup>5</sup>Department of Computational Biomedicine, Cedars Sinai Medical Center, West Hollywood, USA. <sup>6</sup>Data used in preparation of this article were obtained from the Alzheimer's Disease Neuroimaging Initiative (ADNI) database (adni.loni.ucla.edu). As such, the investigators within the ADNI contributed to the design and implementation of ADNI and/or provided data, but did not participate in analysis or writing of this report. A complete listing of ADNI investigators can be found at: http://adni.loni.usc.edu/wp-content/uploads/how\_to\_apply/ADNI\_Acknowledgement\_List.pdf.

#### References

- Jansen, I.E., Savage, J.E., Watanabe, K., Bryois, J., Williams, D.M., Steinberg, S., Sealock, J., Karlsson, I.K., Hägg, S., Athanasiu, L., et al.: Genome-wide meta-analysis identifies new loci and functional pathways influencing alzheimer's disease risk. Nature genetics 51(3), 404–413 (2019)
- Association, A., et al.: 2020 alzheimer's disease facts and figures. Alzheimer's & Dementia 16(3), 391–460 (2020)
- Gatz, M., Reynolds, C.A., Fratiglioni, L., Johansson, B., Mortimer, J.A., Berg, S., Fiske, A., Pedersen, N.L.: Role of genes and environments for explaining alzheimer disease. Archives of general psychiatry 63(2), 168–174 (2006)
- Kunkle, B.W., Grenier-Boley, B., Sims, R., Bis, J.C., Damotte, V., Naj, A.C., Boland, A., Vronskaya, M., Van Der Lee, S.J., Amlie-Wolf, A., et al.: Genetic meta-analysis of diagnosed alzheimer's disease identifies new risk loci and implicates aβ, tau, immunity and lipid processing. Nature genetics 51(3), 414–430 (2019)
- Lambert, J.-C., Ibrahim-Verbaas, C.A., Harold, D., Naj, A.C., Sims, R., Bellenguez, C., Jun, G., DeStefano, A.L., Bis, J.C., Beecham, G.W., et al.: Meta-analysis of 74,046 individuals identifies 11 new susceptibility loci for alzheimer's disease. Nature genetics 45(12), 1452–1458 (2013)
- Shen, L., Thompson, P.M.: Brain imaging genomics: Integrated analysis and machine learning. Proc IEEE Inst Electr Electron Eng 108(1), 125–162 (2020). doi:10.1109/JPROC.2019.2947272
- Fan, C.C., Smeland, O.B., Schork, A.J., Chen, C.-H., Holland, D., Lo, M.-T., Sundar, V., Frei, O., Jernigan, T.L., Andreassen, O.A., et al.: Beyond heritability: improving discoverability in imaging genetics. Human molecular genetics 27(R1), 22–28 (2018)
- Shen, L., Kim, S., Risacher, S.L., Nho, K., Swaminathan, S., West, J.D., Foroud, T., Pankratz, N., Moore, J.H., Sloan, C.D., et al.: Whole genome association study of brain-wide imaging phenotypes for identifying quantitative trait loci in mci and ad: A study of the adni cohort. Neuroimage 53(3), 1051–1063 (2010)
- Weiner, M.W., Veitch, D.P., Aisen, P.S., Beckett, L.A., Cairns, N.J., Green, R.C., Harvey, D., Jack, C.R., Jagust, W., Liu, E., Morris, J.C., Petersen, R.C., Saykin, A.J., Schmidt, M.E., Shaw, L., Shen, L., Siuciak, J.A., Soares, H., Toga, A.W., Trojanowski, J.Q., Alzheimer's Disease Neuroimaging, I.: The alzheimer's disease neuroimaging initiative: a review of papers published since its inception. Alzheimers Dement 9(5), 111–94 (2013)
- Camus, V., Payoux, P., Barré, L., Desgranges, B., Voisin, T., Tauber, C., La Joie, R., Tafani, M., Hommet, C., Chételat, G., et al.: Using pet with 18 f-av-45 (florbetapir) to quantify brain amyloid load in a clinical environment. European journal of nuclear medicine and molecular imaging 39(4), 621–631 (2012)
- 11. Clark, C.M., Schneider, J.A., Bedell, B.J., Beach, T.G., Bilker, W.B., Mintun, M.A., Pontecorvo, M.J., Hefti, F., Carpenter, A.P., Flitter, M.L., et al.: Use of florbetapir-pet for imaging  $\beta$ -amyloid pathology. Jama **305**(3), 275–283 (2011)

 Efthymiou, A.G., Goate, A.M.: Late onset alzheimer's disease genetics implicates microglial pathways in disease risk. Molecular neurodegeneration 12(1), 1–12 (2017)

- Gjoneska, E., Pfenning, A.R., Mathys, H., Quon, G., Kundaje, A., Tsai, L.-H., Kellis, M.: Conserved epigenomic signals in mice and humans reveal immune basis of alzheimer's disease. Nature 518(7539), 365–369 (2015)
- Rathore, N., Ramani, S.R., Pantua, H., Payandeh, J., Bhangale, T., Wuster, A., Kapoor, M., Sun, Y., Kapadia, S.B., Gonzalez, L., et al.: Paired immunoglobulin-like type 2 receptor alpha g78r variant alters ligand binding and confers protection to alzheimer's disease. PLoS genetics 14(11), 1007427 (2018)
- Yan, Y., Zhao, A., Qui, Y., Li, Y., Yan, R., Wang, Y., Xu, W., Deng, Y.: Genetic association of fermt2, hla-drb1, cd2ap, and ptk2b polymorphisms with alzheimer's disease risk in the southern chinese population. Frontiers in aging neuroscience 12, 16 (2020)
- Marioni, R.E., Harris, S.E., Zhang, Q., McRae, A.F., Hagenaars, S.P., Hill, W.D., Davies, G., Ritchie, C.W., Gale, C.R., Starr, J.M., et al.: Gwas on family history of alzheimer's disease. Translational psychiatry 8(1), 1–7 (2018)
- 17. Karch, C.M., Ezerskiy, L.A., Bertelsen, S., (ADGC), A.D.G.C., Goate, A.M.: Alzheimer's disease risk polymorphisms regulate gene expression in the zcwpw1 and the celf1 loci. PloS one 11(2), 0148717 (2016)
- Kikuchi, M., Hara, N., Hasegawa, M., Miyashita, A., Kuwano, R., Ikeuchi, T., Nakaya, A.: Enhancer variants associated with alzheimer's disease affect gene expression via chromatin looping. BMC medical genomics 12(1), 1–16 (2019)
- Han, Z., Huang, H., Gao, Y., Huang, Q.: Functional annotation of alzheimer's disease associated loci revealed by gwass. PloS one 12(6), 0179677 (2017)
- Farfel, J.M., Yu, L., Buchman, A.S., Schneider, J.A., De Jager, P.L., Bennett, D.A.: Relation of genomic variants for alzheimer disease dementia to common neuropathologies. Neurology 87(5), 489–496 (2016)
- Fehér, Á., Juhász, A., Pákáski, M., Janka, Z., Kálmán, J.: Association study of the abca7 rs3752246 polymorphism in alzheimer's disease. Psychiatry research 279, 376–377 (2019)
- Liu, G., Zhang, H., Liu, B., Wang, T., Han, Z., Ji, X.: rs4147929 variant minor allele increases abca7 gene expression and abca7 shows increased gene expression in alzheimer's disease patients compared with controls. Acta neuropathologica 139(5), 937–940 (2020)
- Gong, L., Xu, R., Lan, L., Liu, D., Shen, J., Zhang, B., Initiative, A.D.N., et al.: The cd33 genotype associated cognitive performance was bidirectionally modulated by intrinsic functional connectivity in the alzheimer's disease spectrum. Biomedicine & Pharmacotherapy 115, 108903 (2019)
- Purcell, S., Neale, B., Todd-Brown, K., Thomas, L., Ferreira, M.A., Bender, D., Maller, J., Sklar, P., De Bakker, P.I., Daly, M.J., et al.: Plink: a tool set for whole-genome association and population-based linkage analyses. The American journal of human genetics 81(3), 559–575 (2007)

Kim et al.

Page 8 of 11

### **Figures**

Figure 1 The significance heat map for imaging-diagnosis analysis. The effect of the diagnosis outcome on AV-45 imaging QT data is estimated at each ROI. For each ROI-diagnosis pair,  $-log_{10}(p)$  is color-coded and shown in the heat map.

Figure 2 The distribution of the number of SNPs identified from applying the proposed pipeline to randomly selected 54 SNPs (across 10,000 runs). (a)-(c) show the histograms of the number of SNPs identified for three different diagnostic comparisons (i.e., CN vs AD, CN vs LMCI, and CN vs EMCI) respectively. The red dashed line indicates the number of SNPs identified from the pipeline using 54 AD susceptibility loci.

Figure 3 The significance heat map for imaging-genetics analysis. Sub-figures (a), (b), (c) show the p-value significance of imaging-genetics analysis for all SNP-ROI pairs on three data sets (i.e., CN vs AD, CN vs LMCI, and CN vs EMCI), respectively. For each ROI-SNP pair,  $-log_{10}(p)$  is color-coded and shown in the heat map.

### **Tables**

The tables present in the next page.

### Additional File 1

This file contains the following supplementary table. Supplementary Table S1: The p-value significance for imaging-genetics analysis. Sub-tables (a), (b), (c) show the p-value significance of imaging-geneticsanalysis for all SNP-ROI pairs on three data sets (i.e., CN vs AD, CN vsLMCI, and CN vs EMCI), respectively. For each ROI-SNP pair, the p-value is shown.

Table 1 The comparison of identified genetic variants. We compare the significance of the identified genetic variants using the GWAS, Pearson's correlation, partial correlation, and our model. Corrected-p values are reported in the format of  $-log_{10}(p)$ .

	GWAS			Pearson correlation			Partial correlation			Proposed model		
Gene Symbol-rsID	CN-AD		CN-EMCI		CN-LMCI				CN-EMCI		CN-LMCI	CN-EMC
ADAMTS4-rs4575098	1									1.34	2.69	
CR1-rs6656401	ı									i		
CR1-rs2093760	ı			ı						ı		
CR1-rs4844610				I						I		2.46
BIN1-rs4663105											3.76	
BIN1-rs6733839				-						-	4.50	
INPP5D-rs10933431				-			-			-	1.00	9.24
INPP5D-rs35349669	1										2.00	4.63
CLNK-rs6448453	<u>.</u> I			<u> </u>						2.10	2.00	2.50
MEF2C-AS1-rs190982												2.50
HLA-DRB1-rs9271058	-									1.85	8.37	16.60
CD2AP-rs9473117										1.64	0.51	10.00
CD2AP-rs9381563							-			1.04		
										L		
CD2AP-rs10948363	!			1						2.26		4.40
GPR141-rs2718058										3.26	1 44	4.48
GPR141-rs4723711											1.44	
PILRA-rs1859788										9.00	20.94	
ZCWPW1-rs1476679										7.22	13.40	
NYAP1-rs12539172	1		i							4.20	11.46	
EPHA1-rs10808026	I			ı						I		
EPHA1-AS1-rs7810606				ı						I	4.41	
EPHA1-AS1-rs11771145	ı			l						I	1.71	
PTK2B-rs28834970										7.32		
PTK2B-rs73223431										4.09		
CLU-rs4236673												
CLU-rs9331896	i .									1		
ECHDC3-rs11257238	l			i i						l	5.87	
ECHDC3-rs7920721	I			1						I	2.78	
SPI1-rs3740688										ı		7.72
CELF1-rs10838725	-											4.88
MS4A6A-rs983392				-						1.68		1.00
MS4A2-rs7933202										4.30		
MS4A6A-rs2081545	<u>'</u>			<u> </u>			1			1		
PICALM-rs867611	I			<u> </u>						l I	3.24	3.26
PICALM-rs10792832										·	3.23	3.20
PICALM-1510792032 PICALM-rs3851179											3.23	
FERMT2-rs17125924										ı——	13.22	1.91
FERMT2-rs17125944											15.63	3.06
SLC24A4-rs10498633												3.00
	<u> </u>			<u> </u>							1.96	
SLC24A4-rs12881735	1			1							1.85	4.00
SLC24A4-rs12590654										2.58		4.92
ADAM10-rs442495												
KAT8-rs59735493												
SCIMP-rs113260531										4.80		
	I			1							4.44	2.18
ABCA7-rs111278892				1								
ABCA7-rs3752246										4.50	14.55	2.59
ABCA7-rs4147929										3.65	15.87	2.13
PVRL2-rs41289512	2.60			3.56			4.18			24.24	18.77	32.88
CD33-rs3865444										2.77	4.10	3.03
CASS4-rs6024870	1			I						i	5.70	1.54
	I			l						l	3.20	2.61
CASS4-rs7274581										l		-
APOE-rs429358	12.21	3.68		17.94	2.27	5.98	19.92	7.21	3.63	35.87	40.70	34.81

Table 2 The comparison of the identified genetic variants. We compare correlation coefficients of identified genetic variants using Pearson's correlation, partial correlation, and our model. We removed all non-significant genetic variants (corrected-p > 0.05). We also removed GWAS results because it is based on the regression model. Red and blue colors correspond to identified genetic variants with positive and negative correlation coefficients, respectively.

Gene Symbol-rsID	GWAS				earson correla	ation	Partial correlation			Proposed model		
	CN-AD	CN-LMCI	CN-EMCI	CN-AD	CN-LMCI	CN-EMCI	CN-AD	CN-LMCI	CN-EMCI		CN-LMCI	CN-EMC
ADAMTS4-rs4575098	I			i			i			-0.33	-0.39	
CR1-rs6656401	I			I			I			I		
CR1-rs2093760	1			I			I			I		
CR1-rs4844610				I			I			I		0.38
BIN1-rs4663105											-0.43	
BIN1-rs6733839											-0.46	
INPP5D-rs10933431	i											0.59
INPP5D-rs35349669	ı			1			1			1	-0.36	-0.47
CLNK-rs6448453	I			i i			i i			-0.37		-0.39
MEF2C-AS1-rs190982	I			I			I					
HLA-DRB1-rs9271058	1									0.36	0.57	0.72
CD2AP-rs9473117				-			-			-0.35		
CD2AP-rs9381563	1											
	1											
	i I			1			1			-0.42		-0.46
GPR141-rs4723711	Ī			· I			·			0.72	0.34	010
PILRA-rs1859788				1			1			0.58	0.77	
ZCWPW1-rs1476679	-									0.54	0.67	
NYAP1-rs12539172				-			-			0.45	0.63	
EPHA1-rs10808026	1			1			1			0.45	0.03	
EPHA1-AS1-rs7810606	!			<u> </u>			<u> </u>			<u> </u>	0.46	
	1						!			!		
EPHA1-AS1-rs11771145				1			1			0.54	0.35	
PTK2B-rs28834970	·									-0.54		
PTK2B-rs73223431				·			·			-0.45		
CLU-rs4236673	I									1		
CLU-rs9331896	I .			I.			I.			I		
ECHDC3-rs11257238	1			I .			I .			I .	-0.50	
ECHDC3-rs7920721	1			I			I			I	-0.40	
SPI1-rs3740688												-0.55
CELF1-rs10838725												-0.47
MS4A6A-rs983392										0.35		
MS4A2-rs7933202	ı			i			i			0.45		
MS4A6A-rs2081545	I			I			I			i		
PICALM-rs867611	I			I			I			I	-0.42	-0.42
PICALM-rs10792832				1			1			1	-0.41	
PICALM-rs3851179	1										-0.41	
FERMT2-rs17125924	-						-			-	0.67	0.36
FERMT2-rs17125944	-										0.70	0.41
SLC24A4-rs10498633	1			I							-0.36	0.71
SLC24A4-rs12881735	i I			· I			· I			· I	-0.36	
SLC24A4-rs12590654	T.			· I			1			-0.39	0.50	-0.47
ADAM10-rs442495										-0.39		-0.47
KAT8-rs59735493	-			-			-			-		
SCIMP-rs113260531										0.47		
	1									-0.47	0.46	0.07
	!			<u> </u>			!			!	-0.46	-0.37
	1			1			1			0.46	0.60	0.00
ABCA7-rs3752246										0.46	0.69	0.39
ABCA7-rs4147929										0.43	0.71	0.37
PVRL2-rs41289512	<u> </u>			0.22			0.23			0.80	0.74	0.86
CD33-rs3865444	1									-0.40	0.45	-0.41
CASS4-rs6024870	1									1	0.50	0.34
C/ 100 1 1500 1 11 2 1	I			1			1			1	0.41	0.39
CASS4-rs7274581	1											
APOE-rs429358	-	_	-	0.42	0.18	0.26	0.44	0.28	0.20	0.88	0.90	0.88

Table 3 Top 10 significant ROIs from imaging-diagnosis analysis. We examine the spatial effect of diagnosis outcomes (i.e., CN vs. AD, CN vs. LMCI, CN vs. EMCI) on the Av-45 imaging data. The significant level of the diagnostic effect on the ROI is reported in the format of  $-log_{10}(p)$ .

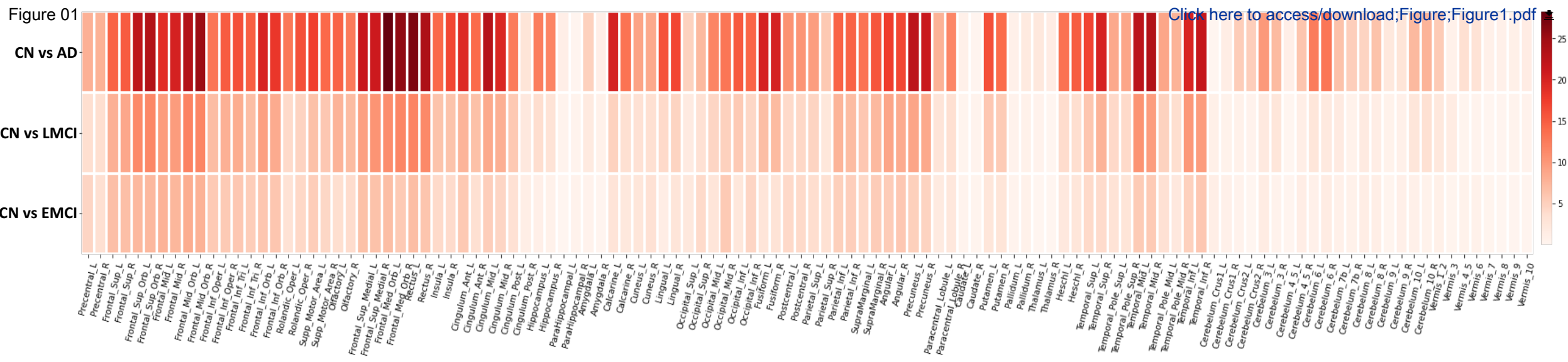
Rank	CN vs. AD		CN vs. LMCI		CN vs. EMCI		
INdIIK	ROI	p-value	ROI	p-value	ROI	p-value	
1	$Frontal\_Med\_Orb\_L$	28.26	$Frontal\_Mid\_Orb\_L$	11.94	Frontal_Mid_Orb_L	8.31	
2	$Rectus_L$	26.92	$Rectus_L$	11.83	$Frontal\_Mid\_Orb\_R$	7.94	
3	$Frontal\_Med\_Orb\_R$	25.86	$Frontal\_Mid\_Orb\_R$	11.78	$Frontal\_Mid\_L$	7.83	
4	$Frontal\_Mid\_Orb\_R$	25.06	$Frontal\_Med\_Orb\_R$	11.63	$Frontal\_Mid\_R$	7.45	
5	$Rectus_R$	23.87	$Frontal\_Sup\_Orb\_R$	11.57	Frontal_Sup_Orb_R	7.36	
6	$Temporal\_Mid\_R$	23.48	$Frontal\_Sup\_Orb\_L$	11.47	Frontal_Sup_Orb_L	7.32	
7	$Frontal\_Mid\_Orb\_L$	23.39	$Rectus_R$	11.38	$Frontal\_Med\_Orb\_L$	6.77	
8	Frontal_Sup_Orb_R	23.37	$Frontal\_Med\_Orb\_L$	11.12	$Rectus_L$	6.75	
9	Cingulum_Mid_L	23.16	$Temporal\_Mid\_L$	10.55	$Frontal\_Sup\_R$	6.70	
10	Temporal_Mid_L	22.73	$Frontal\_Sup\_Medial\_R$	10.39	$Frontal\_Sup\_L$	6.69	

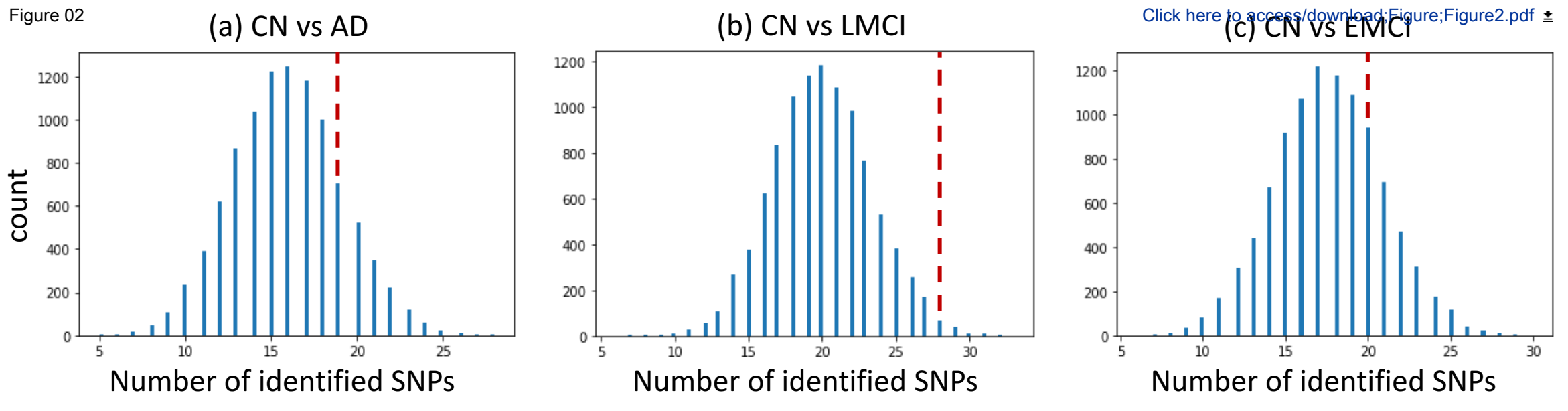
Table 4 Demographic information

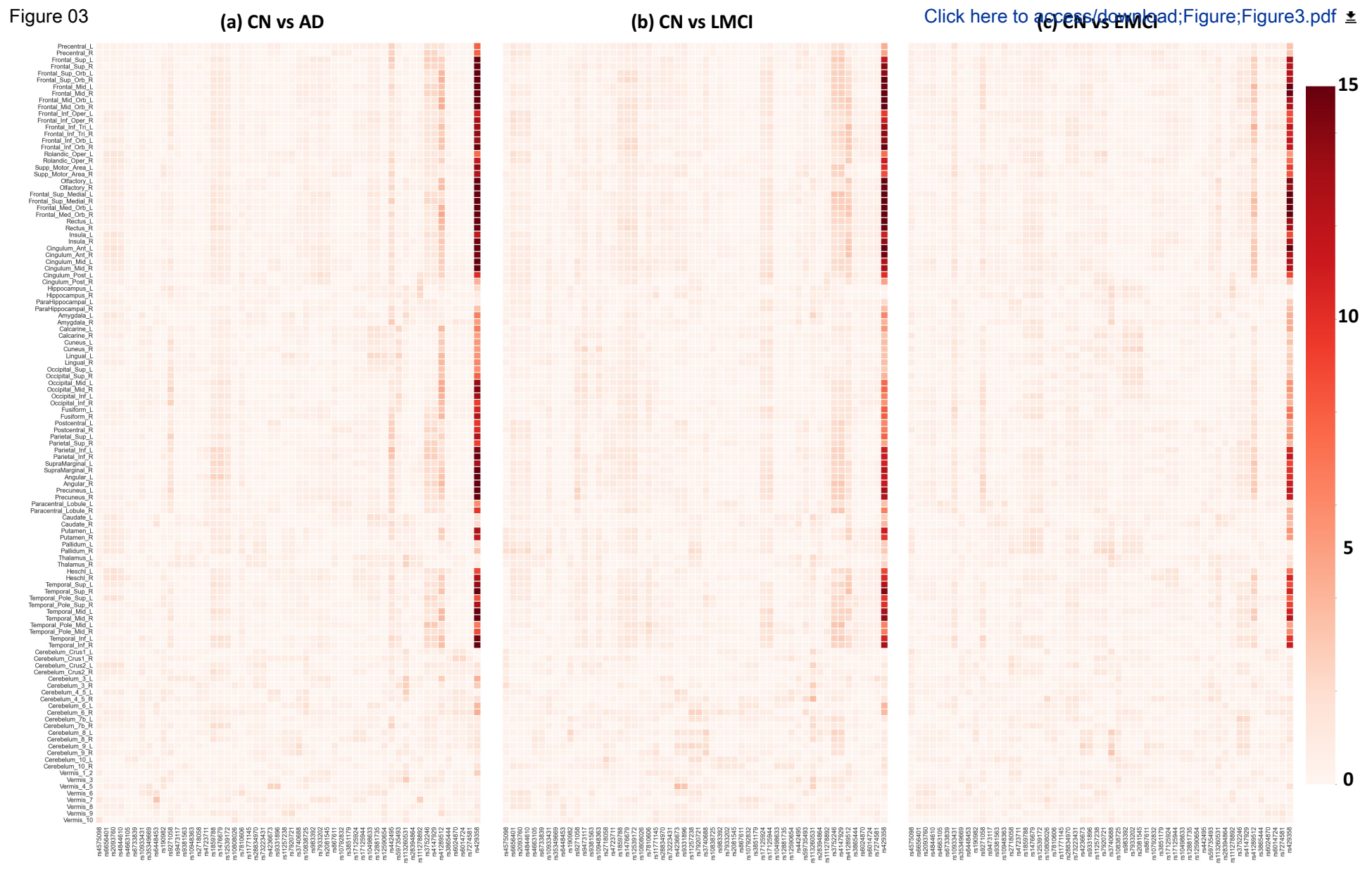
-	CN	EMCI	LMCI	AD	Total
Number of subject	255	296	218	202	971
Age	$76.35 \pm 6.54$	$71.78 \pm 7.28$	$74.71 \pm 8.39$	$75.85 \pm 7.67$	$74.48 \pm 7.67$
Sex (Male/Female)	132/123	167/129	129/89	123/79	551/420
Education (Year)	$16.37 \pm 2.64$	$12.12 \pm 2.64$	$16.12 \pm 2.94$	$15.83 \pm 2.81$	$16.13 \pm 2.75$

Table 5 Selected AD-related SNPs. These include 54 susceptibility loci identified by recent landmark AD genetic studies [1, 4, 5].

rs-ID	Chromosome	Position	Gene Symbol	rs-ID	Chromosome	Position	Gene Symbol
rs4575098	chr1	161155392	ADAMTS4	rs7920721	chr10	11720308	ECHDC3
rs6656401	chr1	207692049	CR1	rs3740688	chr11	47380340	SPI1
rs2093760	chr1	207786828	CR1	rs10838725	chr11	47557871	CELF1
rs4844610	chr1	207802552	CR1	rs983392	chr11	59923508	MS4A6A
rs4663105	chr2	127891427	BIN1	rs7933202	chr11	59936926	MS4A2
rs6733839	chr2	127892810	BIN1	rs2081545	chr11	59958380	MS4A6A
rs10933431	chr2	233981912	INPP5D	rs867611	chr11	85776544	PICALM
rs35349669	chr2	234068476	INPP5D	rs10792832	chr11	85867875	PICALM
rs6448453	chr4	11026028	CLNK	rs3851179	chr11	85868640	PICALM
rs190982	chr5	88223420	MEF2C-AS1	rs17125924	chr14	53391680	FERMT2
rs9271058	chr6	32575406	HLA-DRB1	rs17125944	chr14	53400629	FERMT2
rs9473117	chr6	47431284	CD2AP	rs10498633	chr14	92926952	SLC24A4
rs9381563	chr6	47432637	CD2AP	rs12881735	chr14	92932828	SLC24A4
rs10948363	chr6	47487762	CD2AP	rs12590654	chr14	92938855	SLC24A4
rs2718058	chr7	37841534	GPR141	rs442495	chr15	59022615	ADAM10
rs4723711	chr7	37844263	GPR141	rs59735493	chr16	31133100	KAT8
rs1859788	chr7	99971834	PILRA	rs113260531	chr17	5138980	SCIMP
rs1476679	chr7	100004446	ZCWPW1	rs28394864	chr17	47450775	ABI3
rs12539172	chr7	100091795	NYAP1	rs111278892	chr19	1039323	ABCA7
rs10808026	chr7	143099133	EPHA1	rs3752246	chr19	1056492	ABCA7
rs7810606	chr7	143108158	EPHA1-AS1	rs4147929	chr19	1063443	ABCA7
rs11771145	chr7	143110762	EPHA1-AS1	rs41289512	chr19	45351516	PVRL2
rs28834970	chr8	27195121	PTK2B	rs3865444	chr19	51727962	CD33
rs73223431	chr8	27219987	PTK2B	rs6024870	chr20	54997568	CASS4
rs4236673	chr8	27464929	CLU	rs6014724	chr20	54998544	CASS4
rs9331896	chr8	27467686	CLU	rs7274581	chr20	55018260	CASS4
rs11257238	chr10	11717397	ECHDC3	rs429358	chr19	45411941	APOE
				•			







Supplementary Material

Click here to access/download **Supplementary Material**Additional File 1.xlsx